

pubs.acs.org/joc Article

# Insights into the Mechanism of an Allylic Arylation Reaction via Photoredox-Coupled Hydrogen Atom Transfer

Ethan H. Spielvogel, Bernard G. Stevenson, Michael J. Stringer, Yue Hu, Lisa A. Fredin,\* and John R. Swierk\*



Cite This: J. Org. Chem. 2022, 87, 223-230



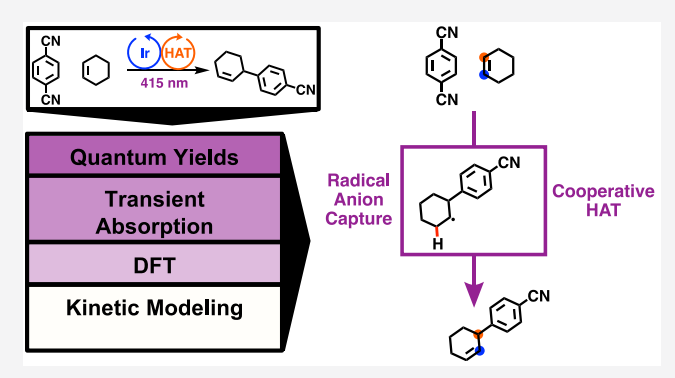
**ACCESS** 

III Metrics & More

Article Recommendations

s Supporting Information

ABSTRACT: Despite widespread use as a synthetic method, the precise mechanism and kinetics of photoredox coupled hydrogen atom transfer (HAT) reactions remain poorly understood. This results from a lack of detailed kinetic information as well as the identification of side reactions and products. In this report, a mechanistic study of a prototypical tandem photoredox/HAT reaction coupling cyclohexene and 1,4-dicyanobenzene (DCB) using an Ir(ppy)<sub>3</sub> photocatalyst and thiol HAT catalyst is reported. Through a combination of electrochemical, photochemical, and spectroscopic measurements, key unproductive pathways and side products are identified and rate constants for the main chemical steps are extracted. The reaction quantum yield was found to decline rapidly over the course of the reaction. An unreported



cyanohydrin side product was identified and thought to play a key role as a proton acceptor in the reaction. Transient absorption spectroscopy (TAS) and quantum chemical calculations suggested a reaction mechanism that involves radical addition of the nucleophilic DCB radical anion to cyclohexene, with cooperative HAT occurring as the final step to regenerate the alkene. Kinetic modeling of the reaction, using rate constants derived from TAS, demonstrates that the efficiency of the reaction is limited by parasitic absorption and unproductive quenching between excited Ir(ppy)<sub>3</sub> and the cyanohydrin photoproduct.

# ■ INTRODUCTION

In recent years, photoredox reactions have rapidly grown in scope and application to small molecule and pharmaceutical synthesis. Photoredox reactions harness the energy in light to generate short-lived excited states, which in turn can undergo electron transfer to initiate a reaction via the generation of a radical intermediate. As an extension, tandem photoredox/organocatalytic methods provide an attractive synthetic approach for the selective activation of stable C–H bonds. This one-pot method leverages both the strong oxidizing and reducing potential of the excited photocatalyst and couples it with an organocatalyst to achieve the desired transformation.

A particularly successful class of tandem photoredox/organocatalytic reactions utilizes hydrogen atom transfer (HAT) catalysts as the co-catalyst. In this context, HAT involves the simultaneous transfer of a proton and electron to generate a reactive radical species, which can then be captured via radical coupling. Thiol HAT catalysts are commonly utilized in tandem photoredox/HAT methods. Most mechanistic proposals involve oxidation of the thiol moiety by the photocatalyst to generate a thiyl radical with the assistance of an ancillary base. These thiyl radicals can then act as potent hydrogen atom abstractors. In the catalysts of tandem photoredox at the catalysts of the photocatalyst to generate a thiyl radical with the assistance of an ancillary base. These thiyl radicals can then act as potent hydrogen atom abstractors.

Despite the importance of tandem photoredox/HAT reactions, the nature of these radical reactions makes their precise mechanism elusive. Nocera and co-workers characterized the mechanism of a photoredox/HAT hydroamidation reaction through transient absorption spectroscopy (TAS), quantum yield (QY) measurements, quenching studies, and DFT calculations.<sup>3</sup> Through their findings, they were able to tune the quantum efficiency of the reaction by modifying the organocatalyst to minimize the rates of deactivation pathways, such as back electron transfer and unproductive HAT. In a more recent study, Knowles and co-workers examined a photoredox-catalyzed anti-Markovnikov radical addition of aminium radical cations to alkenes, which yielded the tertiary amine product.4 By studying the mechanism of the transformation, they were able to identify the source of the hydroamination selectivity as well as which steps in the mechanism limited the overall reaction QY. With this

Received: September 13, 2021 Published: December 9, 2021





knowledge, they were able to tune the HAT catalyst and achieve a significant increase in QY. Other detailed mechanistic studies on photoredox reactions have likewise led to significant improvements in the QY and scope. 8–14

We recently reported on the mechanism of a photoredox-catalyzed  $\alpha$ -aminoarylation reaction involving 1,4-dicyanobenzene (DCB) and N-phenylpyrrolidine. Using TAS and kinetic modeling, we found that the QY of the reaction was limited by light scattering off an insoluble base and parasitic absorption by a ground state donor—acceptor complex between DCB and N-phenylpyrrolidine. The latter limitation was particularly problematic as  $\sim$ 44% of incoming photons are absorbed by the donor—acceptor complex and wasted.

Inspired by our recent work, we report on a related coupling between electron deficient arenes and cycloalkenes to yield allylarenes via a tandem photoredox/HAT reaction originally reported by MacMillan and Cuthbertson (Scheme 1). The

# Scheme 1. Allylic Arylation of Cyclohexene with Tandem Photoredox—HAT Catalysis

+ 
$$\frac{\text{CN}}{\text{K}_2\text{CO}_3, 415 \text{ nm LED}}$$
 CN 2-butanone

allylarene moiety is prevalent in pharmaceutical chemistry and natural product synthesis, making it a particularly attractive candidate for mechanistic studies.  $^{5,16,17}$  In the original mechanistic proposal by MacMillan and Cuthbertson, DCB is reduced by photoexcited  $Ir(ppy)_3$  to generate a radical anion (DCB•-) (Scheme 2). Oxidation and deprotonation of a

# Scheme 2. Original Proposed Mechanism by MacMillan and Cuthbertson<sup>5</sup>

thiol HAT catalyst, Ph<sub>3</sub>SiSH, regenerate the ground state Ir(ppy)<sub>3</sub> and result in a reactive thiyl radical.<sup>5</sup> This thiyl radical is then proposed to abstract a hydrogen from cyclohexene at the allylic position followed by coupling between the neutral cyclohexenyl radical and DCB - with the loss of CN to generate a new C-C bond.<sup>5</sup> In this work, we utilized a combination of TAS and QY measurements to map productive and unproductive reaction pathways and assign rate constants for each step. Electrochemical and NMR binding studies probed the role of the ancillary base, K2CO3, specifically identifying the formation and importance of a previously unrecognized cyanohydrin. Quantum mechanical calculations were utilized to compare the energetics of various mechanisms and pathway intermediates. Finally, kinetic modeling studies demonstrated how parasitic absorption and competitive quenching limit the efficiency of the reaction.

### ■ RESULTS AND DISCUSSION

Steady State Photochemical Studies. Efficient allylic arylation of cyclohexene was achieved at high product yields (87%) and with nearly complete conversion of DCB (~100%) after 24 h of illumination. The maximum product yield was in good agreement with those of MacMillan and Cuthbertson (93%). The discrepancy could be due to differences in the reaction setup, light source, and solvent. The quantum yield of reaction was determined at various points throughout the course of the reaction (Figure 1). A larger margin of error for yield measurements was observed at early times due to quantitative NMR being less sensitive at low concentrations of analyte.

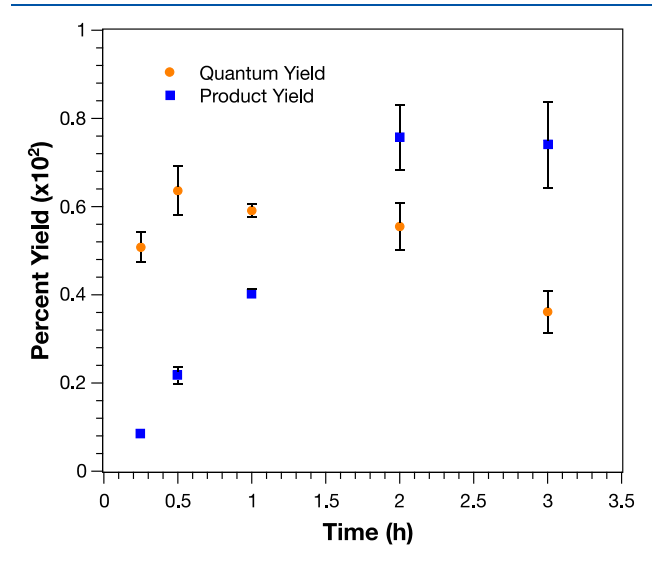


**Figure 1.** Quantum yield of reaction and percent product yield from t = 0 to t = 3 h including standard error for three or four trials.

Over the course of the reaction, the QY ranged from  $\sim 0.60$  at early times to 0.36 at 3 h. Here, the QY of the reaction is defined as the ratio between moles of product and moles of photons absorbed. A QY of between 0.60 and 0.36 is consistent with a non-radical chain mechanism and at early times is on the higher end of these reactions, which often range from 0.02 to 0.50.  $^{3,18-20}$ 

In the absence of  $K_2CO_3$ , the reaction proceeded with a lower product yield (64% after 24 h) but with full conversion of DCB ( $\sim$ 100%).  $K_2CO_3$  is thought to assist in the

deprotonation of Ph<sub>2</sub>SiSH to yield an activated thiyl radical capable of hydrogen atom abstraction.<sup>5</sup> Electrochemically, we observe a shift to a lower oxidation potential for Ph<sub>3</sub>SiSH when in the presence of K<sub>2</sub>CO<sub>3</sub> (Figure S1). However, if K<sub>2</sub>CO<sub>3</sub> is the sole base present and does not regenerate, then the maximum possible yield is 10% as there are only 0.05 equiv of the base in the reaction. This suggests the presence of an additional base, which could be one of the coupling partners or a species generated over the course of the reaction. We observed the formation of 2-butanone cyanohydrin by NMR (Figures S2 and S3) over the course of the reaction, which, we propose, eventually accepts the protons generated in the reaction. 21 Using quantitative <sup>1</sup>H NMR, we plotted the generation of the cyanohydrin over time against the formation of the product (Figure 2). After an initial lag in cyanohydrin formation, it was observed that cyanohydrin formation was tracked with product formation.

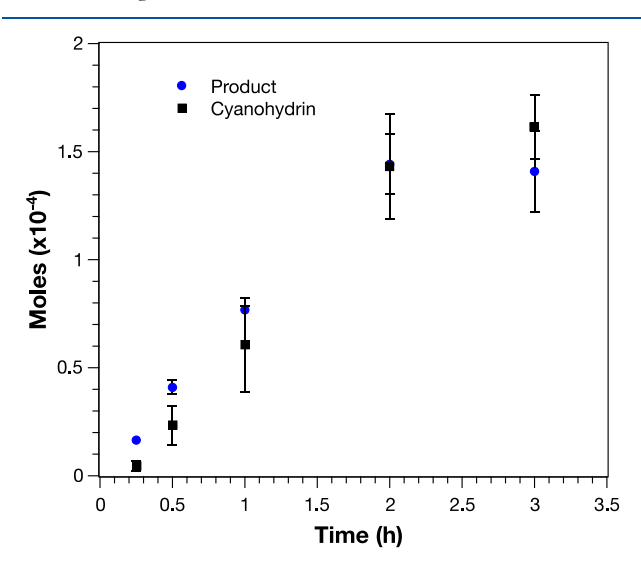


**Figure 2.** Formation of cyanohydrin and product from t = 0 to t = 3 h with standard error among three or four trials.

Though it is clear that the cyanohydrin forms as a result of a 2-butanone reacting with cyanide ions released during the reaction, the precise mechanism of cyanohydrin formation is unclear. In the absence of K<sub>2</sub>CO<sub>3</sub>, the reaction only achieves a 64% product yield and no cyanohydrin is generated. We suggest that under these conditions, cyanide serves as the base and HCN is generated. We attempted to react 2-butanone with potassium cyanide and observed no cyanohydrin formation. Repeating the experiment in the presence of Ir(ppy)<sub>3</sub> and light also did not form cyanohydrin. We also repeated the above studies with potassium bicarbonate and were unsuccessful in generating cyanohydrin. Though the precise mechanism of formation is unclear, taken together, these studies suggest that neither <sup>-</sup>CN nor HCN can be directly trapped by 2-butanone. Instead, a more complex formation mechanism must be at play that is beyond the scope of this study.

Similar to our previous report, we observed a species that absorbs broadly across the visible spectrum when  $Ph_3SiSH$  and  $K_2CO_3$  are mixed (Figures S4 and 5). Though we cannot specify the exact nature of this species, NMR binding studies demonstrate an interaction between  $Ph_3SiSH$  and  $K_2CO_3$  (Figure S6), suggesting that  $K_2CO_3$  may interact with  $Ph_3SiSH$  in the ground state, which could assist in HAT to generate the

thiyl radical. While the molar extinction coefficient at 415 nm of this species is significantly less than that of  $Ir(ppy)_3$ , at the reaction concentration of  $Ph_3SiSH$  and  $K_2CO_3$ , the absorption at 415 nm is sufficiently high to compete with  $Ir(ppy)_3$  for photons. From the absorption spectrum of this species, it was determined that 17.5% of the incoming photons were absorbed by the  $Ph_3SiSH/K_2CO_3$  species instead of  $Ir(ppy)_3$ .

**Electron Transfer Studies.** Stern–Volmer quenching studies were carried out to establish the initial electron acceptor. The rate of quenching for DCB was found to be 1.2  $\times$  10<sup>-9</sup> M<sup>-1</sup> s<sup>-1</sup>, while the rate for Ph<sub>3</sub>SiSH was found to be a  $k_q$  of 5.1  $\times$  10<sup>7</sup> M<sup>-1</sup> s<sup>-1</sup>. The slow quenching rate, combined with the large excess of DCB compared to Ph<sub>3</sub>SiSH, suggest that quenching by the thiol is insignificant. Quenching studies for Ph<sub>3</sub>SiSH in the presence of K<sub>2</sub>CO<sub>3</sub> were unsuccessful due to spectral overlap with Ir(ppy)<sub>3</sub>.

Using TAS, we were able to initiate the reaction and observe the generation of intermediates in real time. Initial electron transfer between excited  $Ir(ppy)_3$  and DCB is clearly demonstrated in the transient absorption spectrum at 200 ns (Figure S8). The transient absorbance at wavelengths longer than 500 nm, as well as the bleach at wavelengths shorter than 400 nm, is a clear indicator for the formation of Ir(IV). The increase in absorption at 440 nm is characteristic of DCB•-. We found that we were able to simulate the transient spectrum by adding together the difference spectra for oxidized  $Ir(ppy)_3$  (3.1  $\mu$ M), DCB•- (3.4  $\mu$ M), and Ph<sub>3</sub>SiS• (0.3  $\mu$ M). The presence of Ph<sub>3</sub>SiS• at early timescales demonstrates efficient oxidation of Ph<sub>3</sub>SiSH by Ir(IV). Kinetic modeling suggests a rate constant of 5  $\times$  10<sup>8</sup> M<sup>-1</sup> s<sup>-1</sup> for this oxidation ( $k_{ox}$ ).

By 1  $\mu$ s, the transient spectrum no longer shows the presence of  $[Ir(ppy)_3]^+$ , suggesting that it has been regenerated via oxidation of Ph<sub>3</sub>SiSH. Instead, we observe a broad absorption feature from 400 to 600 nm and a smaller absorption feature from 700 to 900 nm (Figure 3). Much of

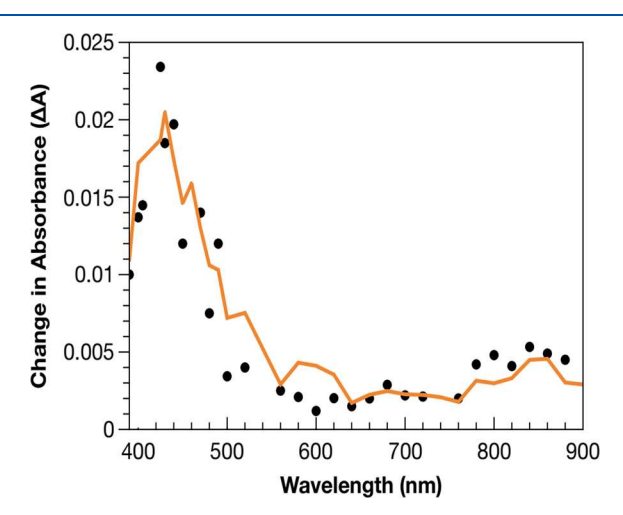


Figure 3. Change in absorption at 1  $\mu s$  (black dots) and sum of difference spectra (orange line) for 3.4  $\mu M$  DCB $\bullet$ -, 3.1  $\mu M$  Ir(IV), and 0.3  $\mu M$  Ph3SiS $\bullet$ .

the 400–600 nm feature can be assigned to  $Ph_3SiS \bullet$  and  $DCB \bullet -$ , while the absorbance at longer wavelengths is consistent with  $[DCB_2] \bullet -$ . We previously observed that over time  $DCB \bullet -$  converts to  $[DCB_2] \bullet -$ , which is the competent coupling partner. The 1  $\mu$ s transient spectrum could be satisfactorily simulated by adding together the

difference spectra for Ph<sub>3</sub>SiS• (3.4  $\mu$ M), DCB•– (3.08  $\mu$ M), and [DCB<sub>2</sub>]•– (0.32  $\mu$ M).

By 10 ms, the only species we observe is  $Ph_3SiS \bullet$  (Figure S9), which suggests that the consumption of  $DCB \bullet -$  and  $[DCB_2] \bullet -$  occurs on a shorter timescale than the disappearance of  $Ph_3SiS \bullet$ . This is confirmed by the single wavelength traces at 480 nm, specific to  $Ph_3SiS \bullet$ , and 780 nm, specific to  $[DCB_2] \bullet -$  (Figure 4). The absorbance related to  $[DCB_2] \bullet -$ 

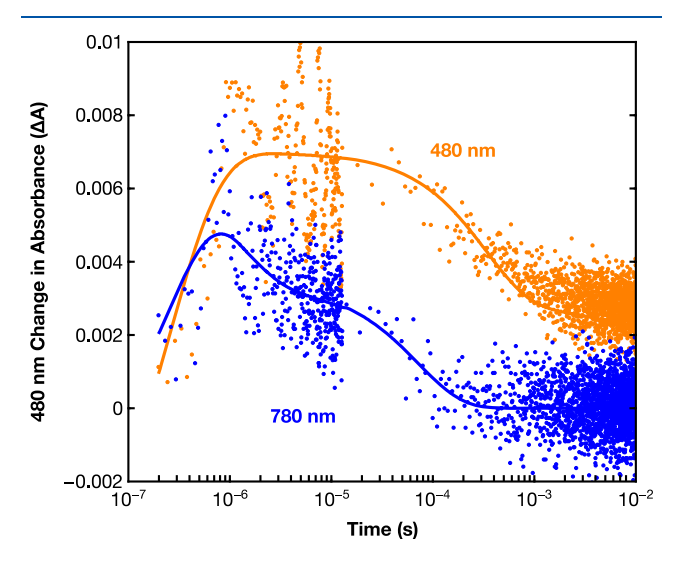
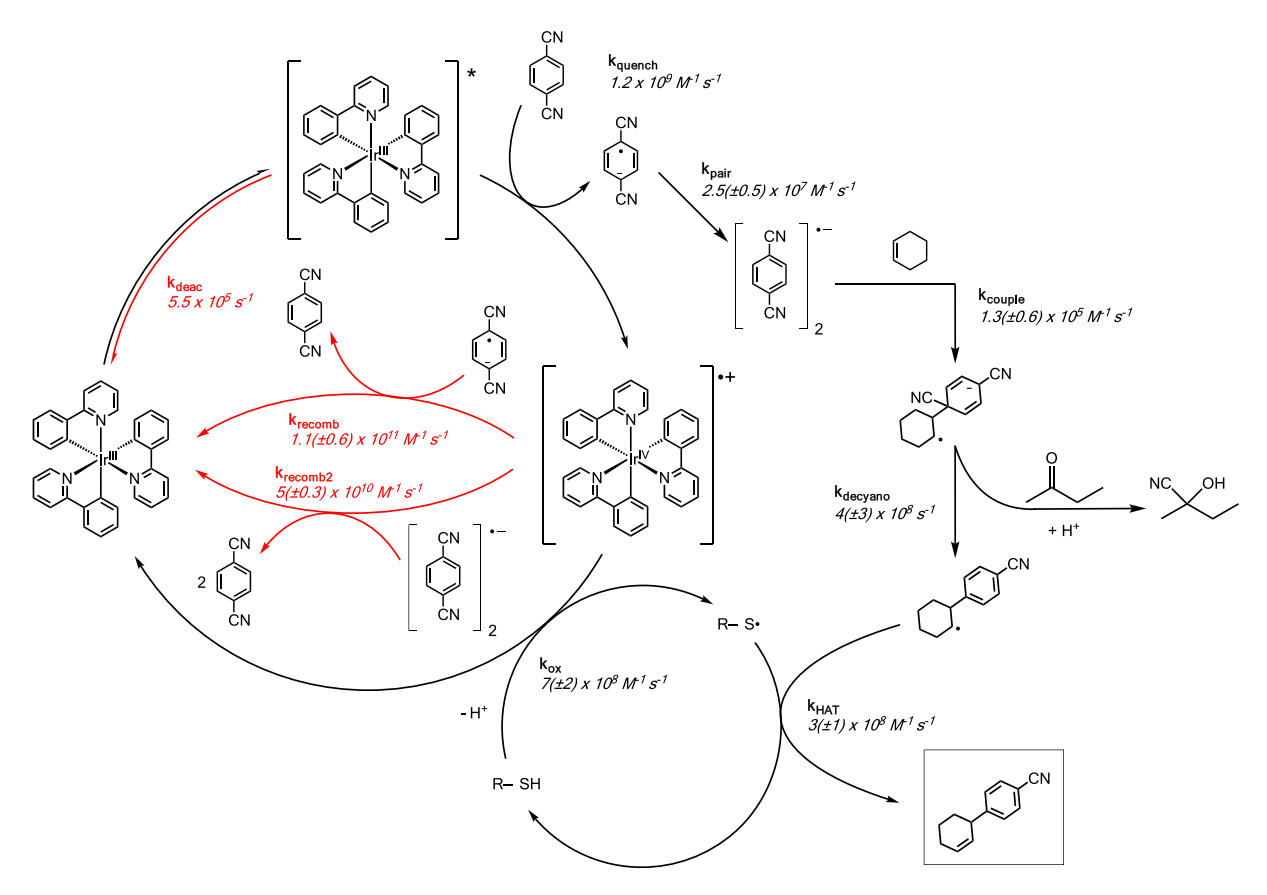


Figure 4. Single wavelength kinetic traces at 480 and 780 nm for various timescales.

is largely gone by 200  $\mu$ s, while the absorbance related to  $Ph_3SiS \bullet$  only begins to decay at that point, suggesting consumption of  $[DCB_2] \bullet -$  before  $Ph_3SiS \bullet$ . In the original mechanistic proposal from Cuthbertson and MacMillan,  $Ph_3SiS \bullet$  abstracts a hydrogen from cyclohexene and then the cyclohexenyl radical and  $DCB \bullet -$  undergo a coupling step. In that case, we would expect the disappearance of  $Ph_3SiS \bullet$  to be either faster or simultaneous with the disappearance of  $[DCB_2] \bullet -$ . Instead, we propose that our data demonstrates that the radical anion is first trapped by cyclohexene via radical addition, with hydrogen abstraction from a radical species occurring as the final step.

In order to probe this hypothesis and extract kinetic information, we developed a kinetic model for the reaction that had the [DCB<sub>2</sub>] • - radical anion first trapped by cyclohexene and hydrogen abstraction occurring afterward. We also observed that it was necessary to include a decyanation step, though the model produces satisfactory results with the decyanation step in place before or after [DCB<sub>2</sub>]•- trapping by cyclohexene. In our model, hydrogen abstraction thus occurs from a radical species in a cooperative HAT step. 22 It is also important to note that in our model, the double bond shifts over by one carbon, which disagrees with the original mechanistic proposal. However, we note that in the original report, use of unsymmetric alkenes produced a variety of isomers, which may be explained by our proposed mechanism.<sup>5</sup> One example of this was the coupling of 1-hexene and DCB, which yielded the arylation product at the 1 position as well as the allylic position.<sup>5</sup> A number of other asymmetric substrates from the original study also resulted in an indistinguishable mixture of isomers. These findings suggest

Scheme 3. Mechanism of Photoredox-Catalyzed Allylic Arylation of Alkenes



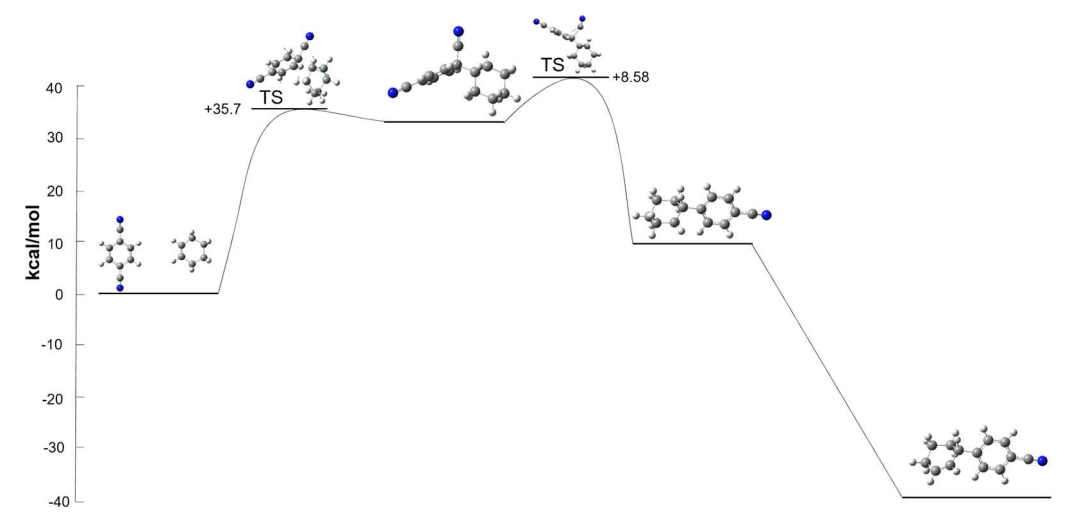


Figure 5. Calculated reaction barriers for the mechanism of photoredox-catalyzed allylic arylation of alkenes. All energies are relative, and full energetics can be found in Table S2. M06-L/6-311g(d,p)/PCM(MeCN)//B3LYP-D3/6-311g(d,p)/PCM(MeCN).

that at least two mechanisms are possible, one where an allylic radical is formed and allows for coupling directly at the allylic position and second where the arene radical adds to the alkene followed by cooperative HAT to regenerate the double bond. In the reaction involving cyclohexene and DCB described in this work, the radical addition mechanism seems to be operative. We cannot rule out that for some alkenes, abstraction of allylic hydrogen before coupling with the arene radical may be preferred for steric or electronic reasons or, that for some substrates, multiple reaction mechanisms may be simultaneously accessible.

The model described above was fit to the single wavelength traces obtained by TAS, with the results shown in Scheme 3. As shown in Figure 4, excellent fits to the experimental data were obtained. Several of the steps involving the DCB•radical anion ( $k_{\text{recomb}}$ ,  $k_{\text{recomb2}}$ , and  $k_{\text{pair}}$ ) are somewhat faster than our previous measurements in dimethylacetamide. 15 This may be the result of the lower polarity 2-butanone affording less stabilization to a charged radical. The value of  $k_{ox}$  that we independently obtained from fitting  $7 (\pm 2) \times 10^8 \,\mathrm{M}^{-1} \,\mathrm{s}^{-1}$  is in excellent agreement with the value predicted by kinetic modeling. Additions of carbon-centered radicals to alkenes have previously been reported in photoredox and related photocatalytic reactions, <sup>23,24</sup> with rate constants on the order  $10^5-10^6$  M<sup>-1</sup> s<sup>-1,25</sup> which is in excellent agreement with the value of  $k_{\text{couple}}$  we determined from fitting (1.3 (± 0.6) × 10<sup>5</sup>  $M^{-1} s^{-1}$ ).

**Quantum Chemistry.** Clarification of the mechanism was achieved through quantum chemical calculations. Structure optimizations were performed in Gaussian16<sup>26</sup> using the hybrid B3LYP functional and a triple- $\zeta$  basis set with polarization. An acetonitrile polarization continuum model of solvation was applied to allow for more charge localization, and GD3 empirical dispersion was used to account for the diffuse  $\pi$ -bonds. Energetics were done with the M06-L functional that provides accurate reaction barriers. Harmonic vibrational frequencies were used to estimate the zero-point energy and the thermal contributions to free energies at 298.15 K as well as to ensure that intermediates were minima on the potential energy surface.

The calculations show that trapping DCBullet by cyclohexene has an  $\sim$ 36 kcal/mol activation energy, which is only 2 kcal/

mol above the resulting intermediate (Figure 5 and Tables S2 and S3). This first step is rate-limiting but well within the type of slow barriers, which are diffusion limited (Table S4). Interestingly this radical trapping transition state is purely driven by electronic interactions between the two molecules and is highly orientation invariant, allowing the DCB - to attack from either side of the cyclohexene. Additionally, the following decyanation step has a relatively low activation barrier (occurring in  $\sim 0.22 \mu s$ , Table S4) and the highly orientation-dependent HAT is barrierless in this mechanism (Figure S10). In comparison, the first two steps of the MacMillan mechanism<sup>5</sup> (Scheme 2, Figure S11, and Tables S2 and S3) feature transition state barriers with at least millisecond timescales (Table S4). In particular, the highly orientation-dependent HAT step is rate-limiting; however, the calculated barrier only captures the electronic energy of the actual moment of hydrogen transfer. For transition states that are highly orientation dependent or have large reorganization energies, the calculated barrier only captures the electronic portion of the kinetics and misses the solution-based interactions, which often drive the measured kinetics. Overall, the computed barriers support the assignment of the observed kinetics with the mechanism proposed in Scheme 3 without ruling out the Scheme 2 mechanism as a possibility for some substrates.

**Kinetic Modeling.** Stochastic modeling software was used to calculate the QY based on the rate constants reported in Scheme 3. The photoredox cycle was modeled by first assuming a constant influx of photons based on the photon flux of the light source used for steady state photolysis measurements.  $Ir(ppy)_3$  was then modeled to absorb a photon of 415 nm light at a fast enough rate to not impact the overall kinetics. Additionally, potassium carbonate was allowed to act as a base twice and the deprotonated cyanohydrin was also allowed to act as a base, all at a rate of  $7.0 \times 10^8 \ M^{-1} \ s^{-1}$ . All other kinetic processes were modeled based on the proposed mechanism in Scheme 3.

Without considering any parasitic absorption or quenching by something other than DCB, the modeled quantum yield was nearly 1.0 until the limiting reagent was fully consumed (Figure S12). This indicates that the inherent kinetics of the reaction are fast enough to convert nearly all absorbed photons

into the product. Competitive quenching was then incorporated into the model by assuming that cyanohydrin could quench the excited photocatalyst via energy transfer at a rate of  $1 \times 10^9 \, \text{M}^{-1} \, \text{s}^{-1}$ . This still gave a QY of nearly 1 at early times (Figure 6, orange trace), with the QY decreasing overtime as

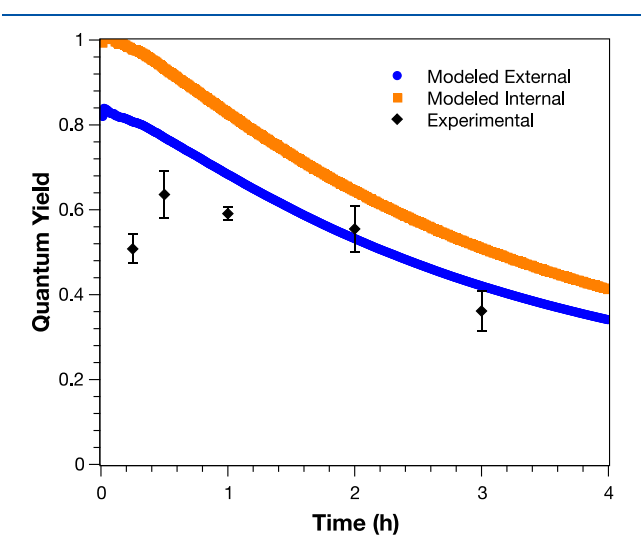


**Figure 6.** Experimental QY and modeled internal and external QY with competitive quenching and parasitic absorption incorporated.

the cyanohydrin concentration increased. Finally, parasitic absorption by the thiol/ $K_2CO_3$  species was accounted for by calculating the QY based on the number of photons absorbed solely by the photocatalyst (Figure 6, blue trace). The result was that the predicted QY matched the experimental data significantly better.

## CONCLUSIONS

Our investigation of an allylic arylation tandem photoredox/ HAT reaction reveals a reaction with an initially high QY that steadily decreases over the course of several hours. NMR studies demonstrate the formation of 2-butanone cyanohydrin, which formed via a reaction between 2-butanone and cyanide anions discharged in the coupling of cyclohexene and DCB. The cyanohydrin in turn appears to play an important role as the terminal base in the reaction. TAS studies and quantum chemical calculations of the reaction suggest a previously unrecognized reaction mechanism where HAT is the final step and occurs via a cooperative HAT mechanism with a radical substrate. Kinetic modeling suggests that kinetics of the reaction are sufficiently fast to allow for a QY near unity but that instead the reaction is limited by parasitic absorption and unproductive quenching by the cyanohydrin.

As with our previous report, the presence of a parasitically absorbing species in this reaction suggests that greater consideration needs to be paid to the impact of unintended reagent absorbances on photoredox reactions. In the case of this reaction, a possible strategy to overcome this may be to shift the wavelength of the light source closer to 400 nm, where the thiol/ $K_2 \text{CO}_3$  species is less absorbing. The use of photocatalysts capable of absorbing in the red would also circumvent this issue and highlights the need for continued development of photocatalysts with a variety of absorption profiles and redox potentials.

While the kinetic modeling suggests that we have identified the majority of the productive and unproductive pathways in this reaction, it is important to mention that there may be other deactivation processes we have yet to identify. These pathways may account for the remaining difference between observed and predicted QY. For example, while most of the  $\rm K_2CO_3$  dissolves in 2-butanone, we observed that some remains undissolved, which could introduce some scattering losses. Likewise, the 100% conversion of DCB with an overall percent yield of 87% implies the existence of a decomposition pathway for DCB that we have not identified. The latter demonstrates the need for continued studies on the stability and decomposition products of cyanoarene radical anions, which are often treated as stable, persistent radicals in reaction design.

#### EXPERIMENTAL PROCEDURE

**General Information.** All reagents except for anhydrous potassium carbonate were obtained from Sigma Aldrich. DCB was crushed with a mortar and pestle prior to use. Cyclohexene was kept under an inert atmosphere and used as received. 2-Butanone was dried over molecular sieves. Triphenylsilanethiol, tetrabutylammonium hexafluorophosphate (TBAPF<sub>6</sub>), and 1,3-bis(trifluoromethyl)-5-bromobenzene were used as received. Anhydrous potassium carbonate was purchased from Alfa Aesar and used as received. NMR spectra were collected using a Bruker Avance III HD 4.

Steady State Photolysis. A stock solution of cyclohexene, triphenylsilanethiol, and 2-butanone was prepared by combining 10 mL of 2-butanone, 1 mmol of cyclohexene (5 equiv), and 0.0097 mmol of triphenylsilanethiol (0.05 equiv). The stock cyclohexene (0.475 M), triphenylsilanethiol (4.83 mM), and 2-butanone solution was degassed for 30 min with nitrogen gas while submerged in an ice water bath. A two-sided quartz screw top cuvette was charged with 0.19 mmol of DCB (1 equiv), 1.9 µmol of tris[2-phenylpyridinato- $C^2$ ,N]iridium(III) (0.01 equiv), and 9.5  $\mu$ mol of potassium carbonate (0.05 equiv), a magnetic stirring flea, and 2 mL of previously degassed cyclohexene/triphenylsilanethiol/2-butanone solution. The combined reaction mixture was degassed for an additional 45 min with nitrogen gas while submerged in an ice water bath. After degassing, the reaction mixture was illuminated for a specified amount of time (0.25-24 h) with a collimated 415 nm LED (Thor Labs M15LP1). Once the illumination time elapsed, 0.25 mmol of internal standard, 1,3bis(trifluoromethyl)-5-bromobenzene, was added to the solution and stirred for an additional 15 min in the dark. Product yields were determined using quantitative HNMR with 1,3-bis(trifluoromethyl)-5-bromobenzene as an internal standard.

The quantum yield of reaction was calculated as follows:

$$\phi_{\text{reaction}} = \frac{n_{\text{product}} N_{\text{A}} hc}{t f P \lambda}$$

where  $n_{\rm product}$  is the product yield,  $N_{\rm A}$  is Avogadro's number (6.022 ×  $10^{23}~{\rm mol^{-1}}$ ), h is Planck's constant (6.626 ×  $10^{-34}~{\rm J\cdot s}$ ), c is the speed of light in a vacuum (2.998 ×  $10^8~{\rm m/s}$ ), f is the fraction of light absorbed at the chosen wavelength with absorbance A ( $f=1-10^{-A}$ ), t is the illumination time in seconds, P is the total power for the detector area (W), and  $\lambda$  is the chosen wavelength (m). The photon flux of the 415 nm LED was determined using a Thorlabs power meter attached to a photodetecting plate with a 1 cm diameter.

**Stern–Volmer Emission Quenching.** Stern–Volmer emission quenching studies were carried out using a Shimadzu RF-6000 Spectrofluorophotometer. The absorbance of each solution was checked prior to collecting emission spectra using the Shimadzu UV-2600 Spectrophotometer to ensure uniformity in concentrations of photocatalysts. A stock solution of 35  $\mu$ M Ir(ppy)<sub>3</sub> was utilized for all experiments. Stern–Volmer experiments were carried out with 150 mM DCB, 100 mM Ph<sub>3</sub>SiSH, and 100 mM Ph<sub>3</sub>SiSH combined with 100 mM K<sub>2</sub>CO<sub>3</sub>. Excitation spectra were collected at an excitation wavelength of 415 nm, and I and I<sub>o</sub> were determined at an emission wavelength of 570 nm.

**Electrochemical Measurements.** Electrochemical measurements were carried out using a BioLogic SP-50 potentiostat and a Pine rotating disk electrode cell with a water jacket. A pseudo-Ag/AgCl reference electrode and gold working electrode were utilized. All measurements were carried out in 0.1 M TBAPF<sub>6</sub> in 2-butanone as an electrolyte. The solvent window was determined prior to experiments with reaction substrates. Cyclic voltammetry was referenced to ferrocene (Fc/Fc<sup>+</sup>). For cyclic voltammetry with triphenylsilanethiol, 0.1462 g of thiol was dissolved in 50 mL of 0.1 M TBAPF6. The potential window was cut off prior to solvent oxidation in order to probe for reversible peaks. Cyclic voltammetry was carried out with equimolar amounts of thiol and  $K_2CO_3$  dissolved in 0.1 M TBAPF<sub>6</sub> in 2-butanone and stirred for 10 min prior to collecting a cyclic voltammogram.

TAS Measurements. Transient absorption spectra were collected using a custom-built spectrometer described in ref 12. An excitation wavelength of 415 nm (1.0 mJ/cm<sup>2</sup>) was used for all experiments. Wavelength traces for the full reaction mixture were collected at wavelengths from 400 to 800 nm and from 200 ns to 10 ms. TAS samples were prepared by combining 100 mM DCB, 5 mM triphenylsilanethiol, 5 mM potassium carbonate, 500 mM cyclohexene, and 3 mL of 35  $\mu$ M Ir(ppy)<sub>3</sub> stock solution in 2-butanone in a four-sided glass screw top cuvette. The cuvette was charged with a magnetic stirring flea and degassed with nitrogen for 1 h while partially submerged in an ice-water bath to prevent evaporation of cyclohexene and 2-butanone. After degassing, the solution was stirred in the dark for 15 min to ensure homogeneity of the reaction mixture. Samples were changed every 2 h, and the stability of each solution was verified by collecting wavelength traces at the same wavelength before and after 2 h.

Kinetic Modeling. Kinetic modeling software Kinetiscope was utilized to create a stochastic model of the reaction (Figure S11). Simulations were set to match concentrations in experimental reactions and contain  $10^8$  particles with  $1.981 \times 10^{-7}$  mol/particle. Equilibrium detect was enabled with a test cycle length of 100 events and a selection frequency of 90.0%. Pressure, volume, and temperature were all set at standard conditions. A constant influx of photons was modeled by allowing a zeroth order reaction to proceed where an arbitrary species W was transformed to hv (symbolizing a 415 nm photon) at a constant rate equal to the moles of photons/s being absorbed by  $Ir(ppy)_3$ .  $Ir(ppy)_3$  was then set to absorb a photon at a rate of  $1 \times 10^{20} \, M^{-1} \, s^{-1}$  as to be essentially instantaneous and not interfere with the overall kinetics of the reaction. Ir(ppy)3\* was modeled to emit an unproductive photon at a rate corresponding to the rate of radiative decay calculated from the phosphorescence lifetime of Ir(ppy)<sub>3</sub>\*. K<sub>2</sub>CO<sub>3</sub> was modeled as being able to act as a base twice due to carbonate having a charge of -2, with both deprotonations occurring at a rate of  $7 \times 10^8 \,\mathrm{M}^{-1} \,\mathrm{s}^{-1}$ . The anionic cyanohydrin was also modeled to deprotonate the thiol in the reaction via PCET with the oxidized photocatalyst at a rate of  $7 \times 10^8 \,\mathrm{M}^{-1} \,\mathrm{s}^{-1}$ . Deprotonation reactions were modeled as being first order in Ph<sub>3</sub>SiSH and Ir(ppy)<sub>3</sub><sup>+</sup> as PCET would likely involve a preassociation of Ph<sub>3</sub>SiSH and K<sub>2</sub>CO<sub>3</sub> or cyanohydrin. The protonated cyanohydrin was modeled to deactivate the excited photocatalyst via energy transfer at a rate of  $1 \times 10^9 \,\mathrm{M}^{-1} \,\mathrm{s}^{-1}$ . A final step was added to allow the excited cyanohydrin to relax back to the ground state at a rate of  $1 \times 10^{10}$  s<sup>-1</sup>. The remainder of the kinetic model was created to represent the mechanism seen in Scheme 3.

**Density Functional Theory.** All calculations were performed using the Gaussian16 program. The relaxed geometries of each molecule was optimized separately using the hybrid B3LYP functional with standard Gaussian type orbital basis sets of triple- $\zeta$  quality with polarization, 6-311G(d,p), with a complete polarizable continuum model (PCM) solvent description of acetonitrile. In addition, dispersion was accounted for using the GD3 correction. Energetics are shown using the M06-L functional, which is known to give good reaction barriers.

**Cyanohydrin Formation Investigations.** Sample mixtures were made using KCN (1.2 mmol) in 3.0 mL of 2-butanone within a sealed two-sided screw top cuvette. Here, 1:1 mole equiv of  $K_2CO_3$ ,

NaHCO<sub>3</sub>, or KHCO<sub>3</sub> to KCN was used. An additional set of samples was prepared in the above way but also with the added  $Ir(ppy)_3$  (3.8  $\mu$ mol). Each separate solution was sparged for 45 min under a nitrogen atmosphere and submerged in an ice bath. The samples were then irradiated with a 415 nm LED for 24 h and analyzed using <sup>1</sup>H NMR to look for formation of cyanohydrin.

# ASSOCIATED CONTENT

# Supporting Information

The Supporting Information is available free of charge at https://pubs.acs.org/doi/10.1021/acs.joc.1c02235.

<sup>1</sup>H and <sup>13</sup>C NMR spectra of relevant compounds, TAS fitting and kinetic modeling parameters, TAS and difference spectra, binding studies data, and quantum chemical studies data (PDF)

# AUTHOR INFORMATION

#### **Corresponding Authors**

Lisa A. Fredin — Department of Chemistry, Lehigh University, Bethlehem, Pennsylvania 18015, United States; oorcid.org/0000-0002-4091-0899; Email: laf218@lehigh.edu

John R. Swierk — Department of Chemistry, State University of New York at Binghamton, Vestal, New York 13850, United States; orcid.org/0000-0001-5811-7285; Email: jswierk@binghamton.edu

#### **Authors**

Ethan H. Spielvogel – Department of Chemistry, State University of New York at Binghamton, Vestal, New York 13850, United States

Bernard G. Stevenson – Department of Chemistry, State University of New York at Binghamton, Vestal, New York 13850, United States

Michael J. Stringer — Department of Chemistry, State University of New York at Binghamton, Vestal, New York 13850, United States

Yue Hu – Department of Chemistry, Lehigh University, Bethlehem, Pennsylvania 18015, United States

Complete contact information is available at: https://pubs.acs.org/10.1021/acs.joc.1c02235

# Notes

The authors declare no competing financial interest.

## ACKNOWLEDGMENTS

This work was supported by the National Science Foundation (award number CHE-2047492). B.G.S. and M.J.S. also thank the Department of Chemistry for summer fellowships. Finally, we wish to acknowledge ChemRxiv for publishing an earlier version of this manuscript as a pre-print.<sup>27</sup>

# **■ REFERENCES**

- (1) Skubi, K. L.; Blum, T. R.; Yoon, T. P. Dual Catalysis Strategies in Photochemical Synthesis. *Chem. Rev.* **2016**, *116*, 10035–10074.
- (2) Qvortrup, K.; Rankic, D. A.; MacMillan, D. W. A General Strategy for Organocatalytic Activation of C–H Bonds via Photoredox Catalysis: Direct Arylation of Benzylic Ethers. *J. Am. Chem. Soc.* **2014**, *136*, 626–629.
- (3) Ruccolo, S.; Qin, Y.; Schnedermann, C.; Nocera, D. G. General Strategy for Improving the Quantum Efficiency of Photoredox Hydroamidation Catalysis. *J. Am. Chem. Soc.* **2018**, *140*, 14926–14937.
- (4) Qin, Y.; Zhu, Q.; Sun, R.; Ganley, J. M.; Knowles, R. R.; Nocera, D. G. Mechanistic Investigation and Optimization of Photoredox

- Anti-Markovnikov Hydroamination. J. Am. Chem. Soc. 2021, 143, 10232–10242.
- (5) Cuthbertson, J. D.; MacMillan, D. W. The direct arylation of allylic sp3 C–H bonds via organic and photoredox catalysis. *Nature* **2015**, *519*, 74–77.
- (6) Becker, P.; Duhamel, T.; Stein, C. J.; Reiher, M.; Muniz, K. Cooperative Light-Activated Iodine and Photoredox Catalysis for the Amination of C<sub>sp3</sub>-H Bonds. *Angew. Chem., Int. Ed.* **2017**, 56, 8004–8008.
- (7) Shaw, M. H.; Shurtleff, V. W.; Terrett, J. A.; Cuthbertson, J. D.; MacMillan, D. W. Native functionality in triple catalytic cross-coupling: sp<sup>3</sup> C-H bonds as latent nucleophiles. *Science* **2016**, *352*, 1304–1308.
- (8) Lewis-Borrell, L.; Sneha, M.; Bhattacherjee, A.; Clark, I. P.; Orr-Ewing, A. J. Mapping the Multi-step Mechanism of a Photoredox Catalyzed Atom-Transfer Radical Polymerization Reaction by Direct Observation of the Reactive Intermediates. *Chem. Sci.* **2020**, *11*, 4475–4481.
- (9) Koyama, D.; Dale, H. J.; Orr-Ewing, A. J. Ultrafast Observation of a Photoredox Reaction Mechanism: Photoinitiation in Organocatalyzed Atom-Transfer Radical Polymerization. *J. Am. Chem. Soc.* **2018**, *140*, 1285–1293.
- (10) Martinez-Haya, R.; Miranda, M. A.; Marin, M. L. Metal-Free Photocatalytic Reductive Dehalogenation Using Visible-Light: A Time-Resolved Mechanistic Study. *Eur. J. Org. Chem.* **2017**, 2017, 2164–2169.
- (11) Rueda-Becerril, M.; Mahé, O.; Drouin, M.; Majewski, M. B.; West, J. G.; Wolf, M. O.; Sammis, G. M.; Paquin, J.-F. Direct C-F Bond Formation Using Photoredox Catalysis. *J. Am. Chem. Soc.* **2014**, *136*, 2637–2641.
- (12) Ting, S. I.; Garakyaraghi, S.; Taliaferro, C. M.; Shields, B. J.; Scholes, G. D.; Castellano, F. N.; Doyle, A. G. <sup>3</sup>d-d Excited States of Ni(II) Complexes Relevant to Photoredox Catalysis: Spectroscopic Identification and Mechanistic Implications. *J. Am. Chem. Soc.* **2020**, 142. 5800–5810.
- (13) Zheng, S.; Zhang, S.-Q.; Saeednia, B.; Zhou, J.; Anna, J. M.; Hong, X.; Molander, G. A. Diastereoselective Olefin Amidoacylation via Pho-toredox PCET/Nickel-Dual Catalysis: Reaction Scope and Mechanistic Insights. *Chem. Sci.* **2020**, *11*, 4131–4137.
- (14) Coles, M. S.; Quach, G.; Beves, J. E.; Moore, E. G. A Photophysical Study of the Sensitization-Initiated Electron Transfer: Insights into the Mechanism of Photoredox Activity. *Angew. Chem., Int. Ed.* **2020**, *59*, 9522–9526.
- (15) Stevenson, B. G.; Spielvogel, E. H.; Loiaconi, E. A.; Wambua, V. M.; Nakhamiyayev, R. V.; Swierk, J. R. Mechanistic Investigations of an  $\alpha$ -Aminoarylation Photoredox Reaction. *J. Am. Chem. Soc.* **2021**, 143, 8878–8885.
- (16) Huang, L.; Rueping, M. Direct Cross-Coupling of Allylic C(sp³)-H Bonds with Aryl- and Vinylbromides by Combined Nickel and Visible-Light Catalysis. *Angew. Chem., Int. Ed.* **2018**, *57*, 10333–10337.
- (17) Pal, S.; Cotard, M.; Géradin, B.; Hoarau, C.; Schneider, C. Cu-Catalyzed Oxidative Allylic C-H Arylation of Inexpensive Alkenes with (Hetero)Aryl Boronic Acids. *Org. Lett.* **2021**, *23*, 3130–3135.
- (18) Xu, W.; Wang, W.; Liu, T.; Xie, J.; Zhu, C. Late-stage trifluoromethylthiolation of benzylic C-H bonds. *Nat. Commun.* **2019**, 10, 4867.
- (19) Dethe, D. H.; Srivastava, A.; Derange, B. D.; Kumar, B. V. Unsymmetrical Disulfide Synthesis through Photoredox Catalysis. *Adv. Synth. Catal.* **2018**, *360*, 3020–3025.
- (20) Lei, Z.; Banerjee, A.; Kusevska, E.; Rizzo, E.; Liu, P.; Ngai, M. Y. β-Selective Aroylation of Activated Alkenes by Photoredox Catalysis. *Angew. Chem., Int. Ed.* **2019**, *58*, 7318–7323.
- (21) Kanda, T.; Naraoka, A.; Naka, H. Catalytic Transfer Hydration of Cyanohydrins to  $\alpha$ -Hydroxyamides. *J. Am. Chem. Soc.* **2019**, *141*, 825–830.
- (22) Kattamuri, P. V.; West, J. G. Cooperative Hydrogen Atom Transfer: From Theory to Application. *Synlett* **2021**, *32*, 1179–1186.

- (23) Rawner, T.; Lutsker, E.; Kaiser, C. A.; Reiser, O. The Different Faces of Photoredox Catalysts: Visible-Light-Mediated Atom Transfer Radical Addition (ATRA) Reactions of Perfluoroalkyl Iodides with Styrenes and Phenylacetylenes. ACS Catal. 2018, 8, 3950–3956.
- (24) Tang, X. J.; Dolbier, W. R. Efficient Cu-catalyzed Atom Transfer Radical Addition Reactions of Fluoroalkylsulfonyl Chlorides with Electron-deficient Alkenes Induced by Visible Light. *Angew. Chem., Int. Ed.* **2015**, *54*, 4246–4249.
- (25) Beckwith, A. L.; Poole, J. S. Factors Affecting the Rates of Addition of Free Radicals to Alkenes-Determination of Absolute Rate Coefficients Using the Persistent Aminoxyl Method. *J. Am. Chem. Soc.* **2002**, *124*, 9489–9497.
- (26) Gaussian 16, Revision C.01, M. J., Frisch; G. W., Trucks; H. B., Schlegel; G. E., Scuseria; M. A., Robb; J. R., Cheeseman; G., Scalmani; V., Barone; G. A., Petersson; H., Nakatsuji; X., Li; M., Caricato; A. V., Marenich; J., Bloino; B. G., Janesko; R., Gomperts; B., Mennucci; H. P., Hratchian; J. V., Ortiz; A. F., Izmaylov; J. L., Sonnenberg; D., Williams-Young; F., Ding; F., Lipparini; F., Egidi; J., Goings; B., Peng; A., Petrone; T., Henderson; D., Ranasinghe; V. G., Zakrzewski; J., Gao; N., Rega; G., Zheng; W., Liang; M., Hada; M., Ehara; K., Toyota; R., Fukuda; J., Hasegawa; M., Ishida; T., Nakajima; Y., Honda; O., Kitao; H., Nakai; T., Vreven; K., Throssell; J. A., Montgomery, Jr.; J. E., Peralta; F., Ogliaro; M. J., Bearpark; J. J., Heyd; E. N., Brothers; K. N., Kudin; V. N., Staroverov; T. A., Keith; R., Kobayashi; J., Normand; K., Raghavachari; A. P., Rendell; J. C., Burant; S. S., Iyengar; J., Tomasi; M., Cossi; J. M., Millam; M., Klene; C., Adamo; R., Cammi; J. W., Ochterski; R. L., Mar-tin; K., Morokuma; O., Farkas; J. B., Foresman; D. J., Fox, Gaussian, Inc., Wallingford CT, 2016.
- (27) Spielvogel, E.; Stevenson, B.; Stringer, M.; Swierk, J. Insights into the Mechanism of an Allylic Arylation Reaction via Photoredox Coupled Hydrogen Atom Transfer. *ChemRxiv*, September 14, 2021, ver. 1. DOI:, DOI: 10.33774/chemrxiv-2021-fh6mj (accessed 2021-11-22).